Proc. Vth International Workshop, Advances in Signal Processing for Non Destructive Evaluation of Materials
Québec City (Canada),2-4 Aug. 2005. © X. Maldague ed., É. du CAO (2006), ISBN 2-9809199-0-X

Keynote lecture

Characterization of Microstructures in Metallic Materials using Static and Dynamic Acoustic Signal Processing Techniques

P. Kalyanasundaram, Baldev Raj and T. Jayakumar
Indira Gandhi Centre for Atomic Research, Kalpakkam 603102, T.N., India

Abstract

In this paper, application of ultrasonic techniques for defect detection in weldments of austenitic stainless steel and maraging steel is discussed. Applications of ultrasonic techniques for characterizing microstructural changes in AISI type 316 stainless steel and modified 9Cr-1Mo ferritic steel; thermomechanical processing of 15Cr-15Ni-2.3Mo-titanium modified austenitic stainless steel (alloy D9) and isothermal annealing behaviour of alloy D9, are discussed. Applications of acoustic emission technique for fatigue crack growth studies in 316 stainless steel and for on-line monitoring of forging of Al alloys are also discussed.

1.0 Introduction

Non-destructive evaluation (NDE) techniques such as ultrasonic and acoustic emission are employed for detection of defects and microstructural characterization in materials. Broadly speaking, while ultrasonic techniques are used for detection of static changes in materials, acoustic emission technique (AET) is used for revealing the dynamic changes occurring in the materials. In this paper, application of ultrasonic techniques for defect detection in weldments of austenitic stainless steel and maraging steel, where detection of defects using ultrasonic testing is a significant challenge because of poor signal to noise ratio of the ultrasonic signals associated with dendritic (hence anisotropic) microstructures of the weldments, has been discussed. Applications of ultrasonic techniques based on time and frequency domain signal analysis for characterizing microstructural changes in materials such as grain size in AISI type 316 stainless steel and modified 9Cr-1Mo ferritic steel, thermomechanical processing of 15Cr-15Ni-2.3Mo-Ti modified austenitic stainless steel (alloy D9), isothermal annealing behaviour of alloy D9, etc. are discussed. Applications of AET for fatigue crack growth studies in parent and weld specimens of AISI type 316 stainless steel and for on-line monitoring of forging of Al alloys, are also discussed.

2.0 Application of Ultrasonic Techniques for Defect Detection in Weldments

Industrial components in many chemical, petrochemical, process and nuclear industries are made of stainless steels. Detection of defects in welds of stainless steel with textured and dendritic structure, using ultrasonic testing poses a great difficulty because of poor signal to noise ratio of the ultrasonic signals. The noise due to grain scattering dominates the signal corresponding to a defect. Therefore, advanced signal analysis concepts such as spectral analysis, pattern recognition and neural network analysis are employed in such cases. Dendritic (hence anisotropic) microstructures of stainless steel weldments, especially in the thickness range of 10 to 40 mm pose problems for ultrasonic testing. Considering these facts, the ASME boiler and presser vessel code has recommended that in the case of austenitic stainless steel weldments, any defect that is 10 % of thickness should be recorded and

monitored. In some cases, it may be desirable to detect defects of less than 10% of the thicknesses. In this connection, signal analysis (SA) procedures, by using effective cluster and pattern analysis algorithms have been developed, in the authors' laboratory [1,2]. These enable detection and characterization of defects down to 1% of weld thickness (14.0 mm weld thickness) in austenitic stainless steel welds. The pattern analysis method generates a pattern called demodulated auto-correlogram (DMAC) from the auto-correlation function of a signal. Features of DMAC are studied for interpretation and evaluation. In Fig.1, ultrasonic signal patterns of typical noise, porosity, notches and cracks in austenitic stainless steel welds are shown [2]. In case of maraging steel weldments used in rocket motor casings by aerospace industry, tight cracks (3 mm X 1 mm) produced by fatigue loading were detected and characterized using cluster and pattern analysis principles (Fig.2). Detection of such small cracks enables in reducing wall thickness of the rocket motor casing and hence in decreasing weight to thrust ratio of the casing. In both the cases, the cluster and pattern analysis methods use the cross-power spectrum (between signals from weld noise (Fig.2a) and those from the defects (Fig.2b)), to obtain the cluster elements.

3.0 Application of Ultrasonic Techniques for Grain Size Measurement

The ultrasonic spectral analysis based methodologies have been developed for grain size measurement in AISI type 316 stainless steel and modified 9Cr-1Mo ferritic steel [3]. Amplitude of ultrasonic signals for different grain sizes and correlation of peak frequency (PF) and frequency at full width half maximum (FWHM) of ultrasonic signals and yield strength with grain size for this steel are shown in Fig.3. For the first time, the importance of spectral characteristics of different ultrasonic transducers has been brought out for assessment of grain size in materials with differing elastic anisotropies and hence different scattering powers. It has been demonstrated that the transducer exhibiting single peak in the autopower spectrum of the first backwall echo should be used for higher scattering materials, such as austenitic stainless steels, whereas the transducer exhibiting double peak should be used for lower scattering materials, such as ferritic steels.

4.0 Characterization of Microstructural Evolution during Thermomechanical Processing of 15Cr-15Ni-2.3Mo-Ti Modified Stainless Steel using Ultrasonic Technique

Ultrasonic velocity and attenuation measurements have been carried out on a 15Cr-15Ni-2.3Mo-titanium modified austenitic stainless steel (alloy D9) after thermomechanical processing. The cylindrical specimens of alloy D9 were subjected to upsetting at 1273 K for various strains in the range of 0.1 to 0.5 in a hydraulic press. The upset samples were then analyzed for microhardness for predicting the extent of recrystallization during processing. The microstructural examination was carried out to obtain the grain sizes of the samples with the processing history. A slice of 4 mm thickness was cut along the forging axis using electric discharge machining for all the test conditions. The upsetting develops dean metal zone, two perpendicular intense shear zones at 45^0 to the loading direction and deformation zone in the specimens. Autopower spectra of the first back wall echoes obtained in slices 0-5 is shown in Fig.4a. While peak frequency and ultrasonic velocity for slices 0-5 are shown in Fig.4b. It has been found that ultrasonic attenuation and spectral analysis of the first back wall echo can be used for the evaluation of grain size, whereas, ultrasonic velocity is mainly influenced by the presence of texture and hence the extent of recrystallization. An important observation made is that the sample upset to a strain of greater than 0.4 resulted in very fine grain size in the intense shear deformation zone. In the sample upset to a strain of 0.5, the ultrasonic attenuation measurements indicated the presence of fine grains in only one intense shear

region, which was later substantiated through metallographic studies. The results bring out the potential of ultrasonic measurements for characterizing the nonuniform deformation due to asymmetry in loading, strain distribution and extent of rectystallization during thermomechanical processing of 15Cr-15Ni-2.3Mo-titanium modified austenitic stainless steel.

5.0 Ultrasonic Velocity Measurements for Characterization of Annealing Behaviour of Cold Worked alloy D9

Ultrasonic velocity measurements using 4MHz shear waves have been carried out on 20% cold worked (tensile pulled) and annealed specimens of alloy D9 to characterize the isothermal annealing behaviour [4]. Shear velocity measurements have been made in all possible directions with reference to cold worked and wave polarization directions. Velocity ratio parameters (VS3-VS2)/VS3, (VS3-VS1)/VS3 and (VS2-VS1)/VS2 were established and plotted against the annealing temperature (Fig.5). In Fig.5, the fraction recrystallised microstructures with annealing is also plotted. In the velocity ratio parameters, VS1 is the shear wave velocity measured parallel to the tensile pulling direction, VS2 is the shear wave velocity measured perpendicular to tensile pulling direction but polarization parallel to pulling direction and VS3 is the velocity perpendicular to tensile pulling direction with wave polarization perpendicular to tensile pulling direction. A velocity parameter (VS3-VS1)/VS3, which is a combination of the shear wave velocities measured in the transverse direction with polarization directions parallel and perpendicular to the cold worked direction was found to closely represent the extent of recrystallization (Fig.5). The velocity measurements could sense the onset, progress and completion of recrystallization more accurately compared with that of hardness and strength measurements. It has been found that the variation in velocity with annealing time is similar at different frequencies (2, 10, 20 MHz) of the ultrasonic waves used for velocity measurements.

6.0 Acoustic Emission Technique (AET) for Fatigue Crack Growth Studies in AISI type 316 Stainless Steel

AET, which gives information on the dynamic changes such as plastic deformation and crack propagation, can be applied for continuous monitoring of fatigue crack growth (FCG) [5]. During FCG, the major source of AE for a ductile material could be the cyclic plasticity occurring ahead of the crack tip, whereas, for brittle materials, the crack extension at the crack tip could be the major source of AE. Apart from this, the presence of second phase precipitates, inclusions, residual stress induced microcracking in weld structure etc. can significantly influence the AE activity during fatigue crack growth.

Acoustic emission behaviour during fatigue crack growth (FCG) in parent and weld specimens of AISI type 316 stainless steel has been studied. Variation in cumulative ringdown counts (N) and crack growth rate (da/dn) as a function of cyclic stress intensity factor (ΔK) for 25 mm thick solution annealed (SA) and thermally aged (TA) specimens of 316 stainless steel has been shown in Fig.6. AET can be applied to distinguish the transition from sub stage IIa to IIb during stage II FCG by observing a sharp decrease in AE activity in both parent and weld specimens. The transition point in the cumulative ringdown count vs ΔK plot coincides with the da/dn vs ΔK plot. The AE activity increases with increase in ΔK during stage IIa and decreases during stage IIb. The increase in the AE activity with increase in ΔK during stage IIa is attributed to the increase in the size of the cyclic plastic zone (CPZ) which is generated and developed only under plane strain conditions. The decrease in the AE

activity during stage IIb is attributed to the decrease in the size of the CPZ under plane stress conditions. The higher AE activity during the substage IIa is attributed to irreversible cyclic plasticity with extensive multiplication and rearrangement of dislocations taking place within the CPZ.

7.0 Acoustic Emission Technique for Monitoring of Forging Processes

AE monitoring of hot forging processes of aluminium alloys has been carried out. With the optimized sensor location at bottom die of the forging press, AE signals generated during open die and closed die forging operations of a number of workpieces of Al alloy were recorded. The results have shown that the forging processes are characterized by three stages: (i) an initial rapid increase in the AE due to generation and movement of dislocations, (ii) a decrease in the AE thereafter and (iii) a significant increase in the AE beyond a specific time due to die filling which promotes increased friction between the die and the workpiece material (Fig.7). Studies carried out on the effect of lubrication during open die forging showed that AE generation increases with decrease in lubrication in the workpiece.

8.0 Summary

Applications of signal analysis on ultrasonic signals for defect detection and microstructural characterization in austenitic and ferritic steels have been discussed. Applications of acoustic emission technique for fatigue crack growth studies in 316 stainless steel and on-line monitoring of forging of Al alloys have also been discussed. These studies point to possibilities of finding robust solutions for characterization of conventional processes and components, based on judicious selection of parameters of the techniques and appropriate signal analysis methodologies.

Acknowledgements

Authors are thankful to many colleagues, specifically Dr. C.K. Mukhopadhyay and Dr. Anish Kumar in the Non Destructive Evaluation Division of Indira Gandhi Centre for Atomic Research for their contributions.

References

1. P. Kalyanasundaram, Baldev Raj, P. Barat and T. Jayakumar, ‘Reliability of Detection of Small Defects in Noisy Weldments by Advanced Signal Processing and Pattern Recognition Techniques’, Int. J of Press. Vess. & Piping, Vol. 36, 1989, p.103.
2. P. Kalyanasundaram, C. Rajagopalan, Baldev Raj, O. Prabhakar and D.G.R. Sharma, ‘High Sensitivity Detection and Classification of Defects in Austenitic Weldments using cluster Analysis and Pattern Recognition’, Brit. J. of NDT, Vol. 33, 1991, p.290.
3. Anish Kumar, Jayakumar, T., and Baldev Raj, ‘Ultrasonic Spectral Analysis for Microstructural Characterization of Austenitic and Ferritic Steels’, Philosophical Magazine A, Vol. 80, 2000, pp.2469-2487.
4. P. Palanichamy, M. Vasudevan, T. Jayakumar, S. Venugopal and B. Raj, ’Ultrasonic Velocity Measurements for Characterizing the Annealing Behaviour of Cold Worked Austenitic Stainless Steel’, NDT & E International, Vol. 33, 2000, pp.253-259 .
5. V. Moorthy, T. Jayakumar and Baldev Raj, Bull. Mater. Sci., Vol. 17, 1994, pp.699-715.

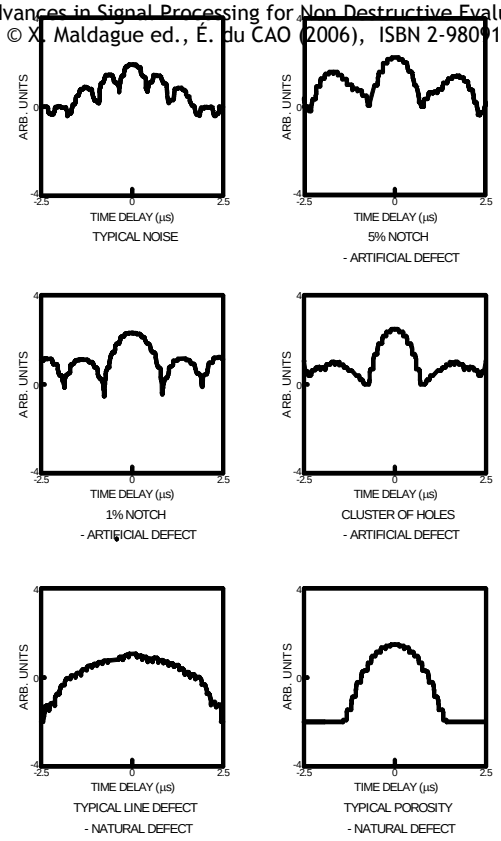

Fig. 1 Ultrasonic signal patterns of typical noise, porosity, notches and cracks in austenitic stainless steel welds.

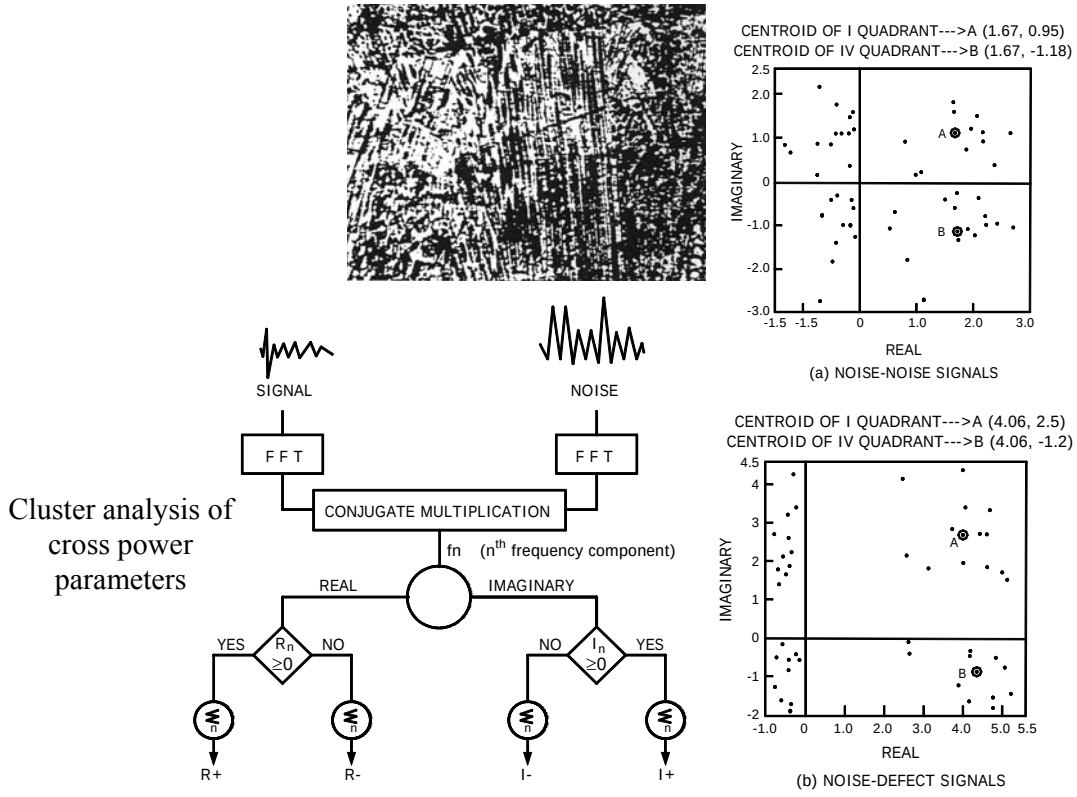

Fig.2 Detection of cracks in Maraging steel weldments

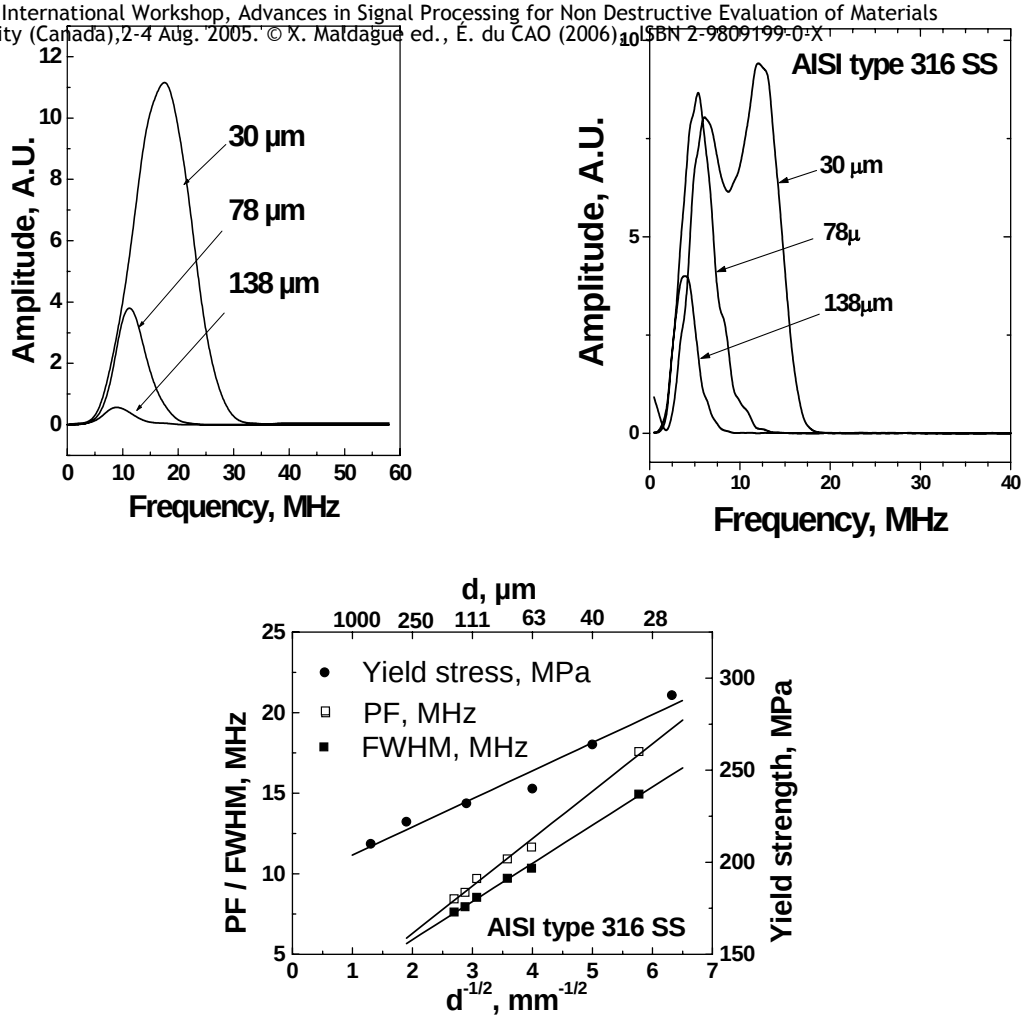

Fig. 3 Grain size measurement in AISI type 316 stainless steel

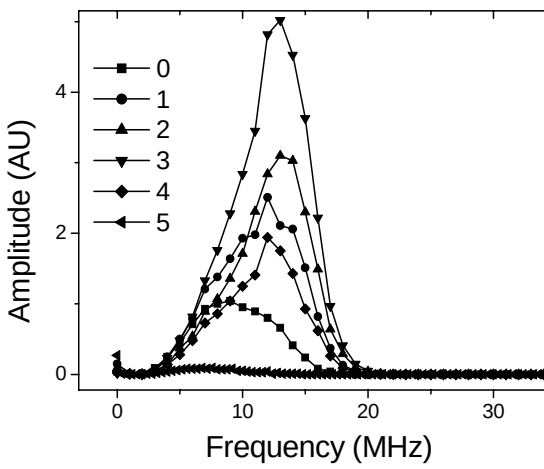

Fig. 4a Autopower spectra of the first back wall echoes obtained in slices 0-5.

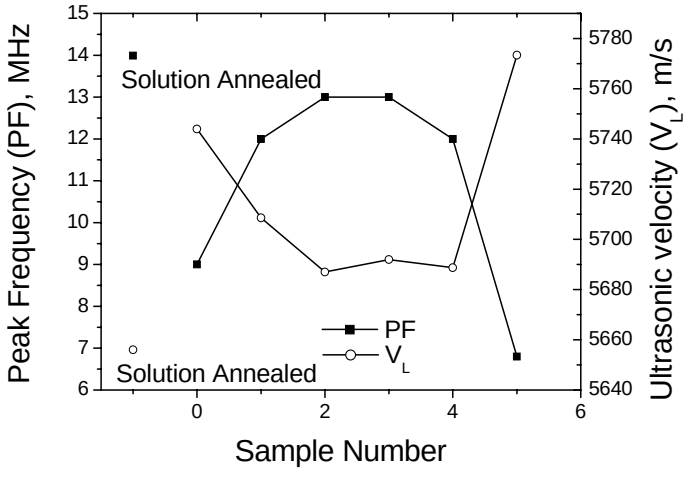

Fig. 4b Peak frequency and Ultrasonic velocity for slices 0-5.

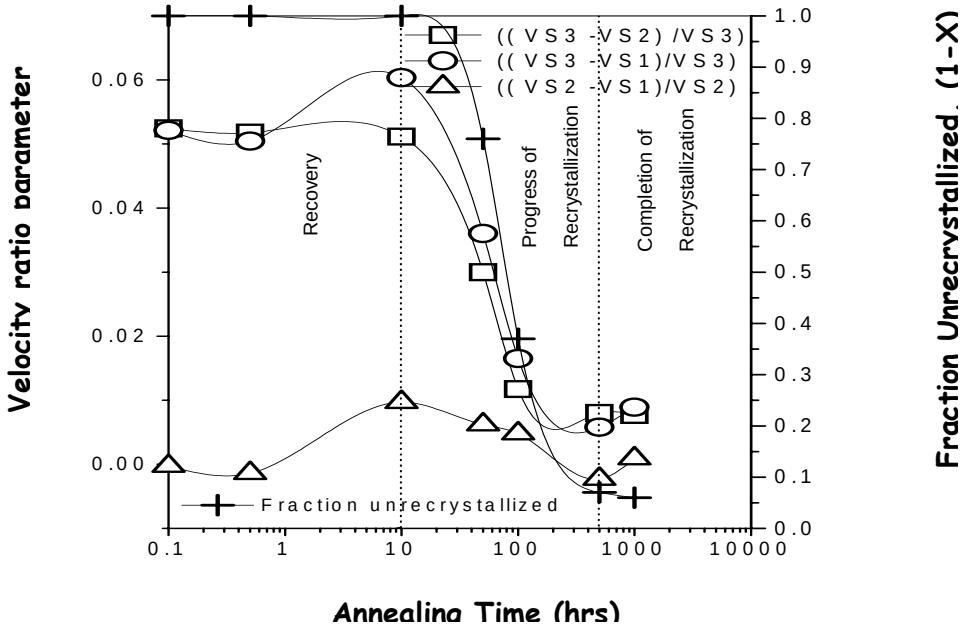

Fig.5. Variation in velocity ratio parameter and fraction recrystallised microstructures with annealing

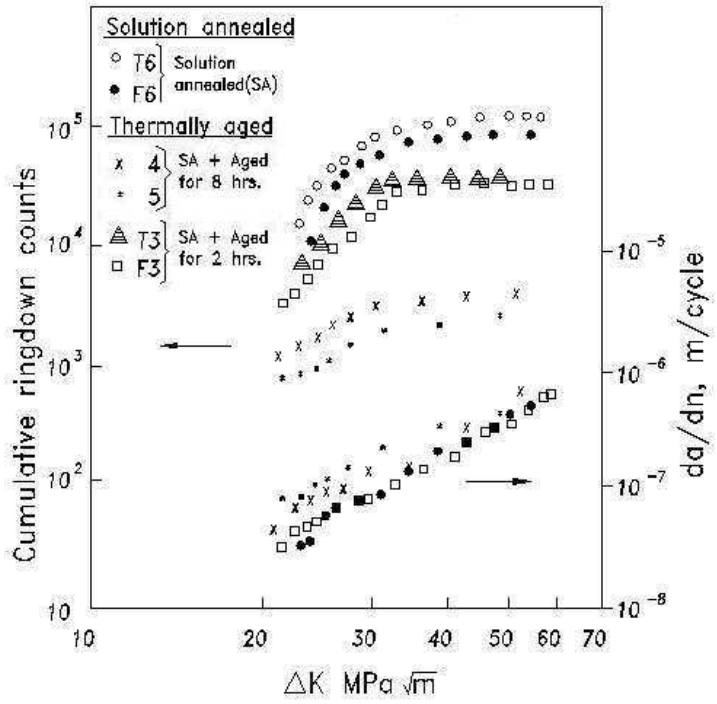

Fig.6. Variation in cumulative ringdown counts (N) and crack growth rate (da/dn) as a function of cyclic stress intensity factor (ΔK) for 25 mm thick solution annealed (SA) and thermally aged (TA) specimens of 316 stainless steel.

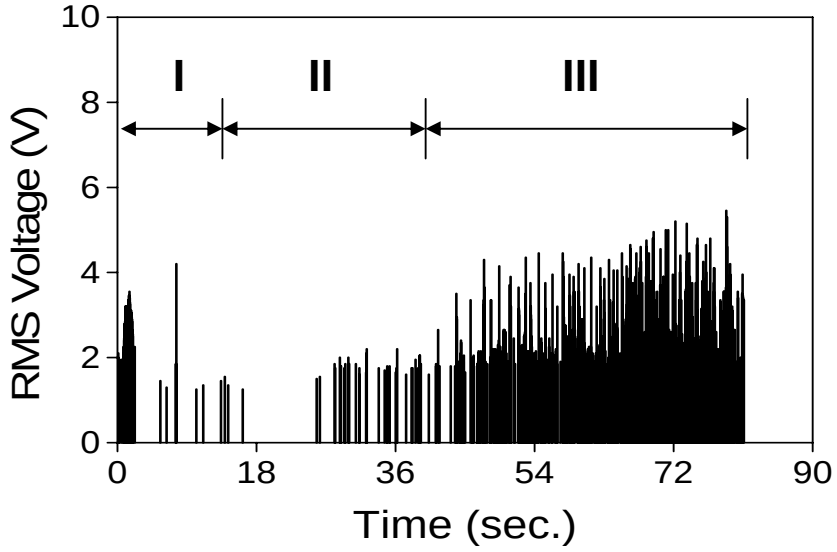

Fig. 7 Acoustic Emission during Open Die Forging of Al Alloy.

Proc. Vth International Workshop, Advances in Signal Processing for Non Destructive Evaluation of Materials
Québec City (Canada),2-4 Aug. 2005. © X. Maldague ed., É. du CAO (2006), ISBN 2-9809199-0-X

Thickness and grain size monitoring in seamless tube making process using laser-ultrasonics

by D. Lévesque[1], S.E. Kruger[1], G. Lamouche[1], R. Kolarik II[2], G. Jeskey[3], M. Choquet[4] and J.-P. Monchalin[1]

[1]Industrial Materials Institute, National Research Council of Canada, Boucherville, Qc, J4B 6Y4, Canada; [2]The Timken Company, R&D Materials, Canton, Ohio, 44706-0930, USA; [3]Jeskey Consulting, Union town, 44685, Ohio, USA; [4]Tecnar Automation Ltée., St-Bruno, Qc, J3V 6B5, Canada

Abstract

The seamless tube making process oftentimes causes wall thickness variations generally in a helical pattern along the tube length. A laser-ultrasonic system installed immediately after the final operation in tube making provides process monitoring. Tube wall thickness and temperature measurements guide the mill adjustments to achieve the desired tolerances. Using the same ultrasonic signals, additional functionality provides the ability to measure the size of austenite grains. A signal processing approach based on a single echo analysis is used for determining wall thickness and austenitic grain size in relatively thick materials. Discussions review challenges specific to on-line conditions such as limited signal-to-noise ratio. A statistical comparison with metallographic results shows that the laser-ultrasonic grain sizes determined on-line have at least the same accuracy.

Keywords: thickness, austenite grain size, laser-ultrasonics, seamless tube

1. Introduction

Seamless tubes are used for numerous applications, such as hydraulic cylinders and power transmission components (gears and bearing races), where microstructural variation due to a weld seam is not acceptable. The seamless tube making process can cause wall thickness variations, which often follow a helical pattern. Thickness measurements during the production is not easy, firstly because of the relatively high tube temperature (of about 1000 °C), and secondly because the tube is not precisely guided.

Laser-ultrasonics [1], which uses lasers for the generation and detection of ultrasound at a distance, was the elected technique to develop the mill-worthy system. Although there has been previous in-plant demonstration of this technique for on-line tube gauging [2-4], this is the first system continuously used in production. Using the same ultrasonic signals, added functionality provided the ability to measure the size of the austenite grains, which largely determine the final microstructure, and consequently the mechanical properties of steels. While the time propagation of an ultrasonic echo can provide information about the thickness of the tube, ultrasonic attenuation can provide information about the grain size in the austenitic phase [5], which is the standard phase for hot-rolling steel products. Continuous in-line monitoring of grain size facilitates a controlled process that leads to an optimized microstructure, avoiding post-production modifications usually performed through costly heat treatments.

After a brief description of the system, the paper presents the signal processing approaches involved in the measurements of wall thickness and austenitic grain size using a single echo and a reference, for use in relatively thick materials (up to 30 mm). Discussions review the challenges specific to on-line conditions, in particular limited signal-to-noise ratio. The laser-ultrasonic system, which has been running at The Timken Company in Ohio, USA, for more than three years, is performance evaluated for the continuous monitoring of both wall thickness and austenite grain size.

2. Description of the system

Generation of ultrasound is performed in the ablation regime by a sufficiently strong laser pulse. The recoil effect following material ejection off the surface (essentially surface oxide) and plasma pressure produces strong longitudinal (compressional) ultrasonic wave emission perpendicular to the surface. The ultrasonic waves, after reflection by the inner wall of the tube, cause a small surface motion on the outer surface (see Figure 1a). Detection of the ultrasound uses a second laser with pulse duration sufficiently long to capture the ultrasonic signal of interest. The surface motion associated with the arrival of the ultrasonic signal produces a Doppler frequency shift on the scattered light that is demodulated by an optical interferometer. Figure 1b shows an ultrasonic signal obtained on-line on a steel tube at high temperature. Specially designed laser Doppler velocimeters (translation and rotation) and two-color pyrometer allow the measurement of the position and temperature at the measurement location (see Ref. 6 for details). An off-line cabin houses the laser-ultrasonic system including all delicate equipments (lasers, interferometer, etc.) in a clean air-conditioned environment. Optical fibers transmit the light beams for the three functions (laser-ultrasonics, pyrometry and velocimetry) to a front coupling probe located right on the production line. The lasers include the generation short-pulsed Nd:YAG laser and the detection laser, which is long-pulse Nd:YAG with a high frequency stability. The repetition rate is 100 Hz, which gives, depending upon the processing conditions and the tube outer diameter, 5 to 15 data points per tube circumference. The demodulator is a stabilized confocal Fabry-Perot interferometer also located inside the cabin.

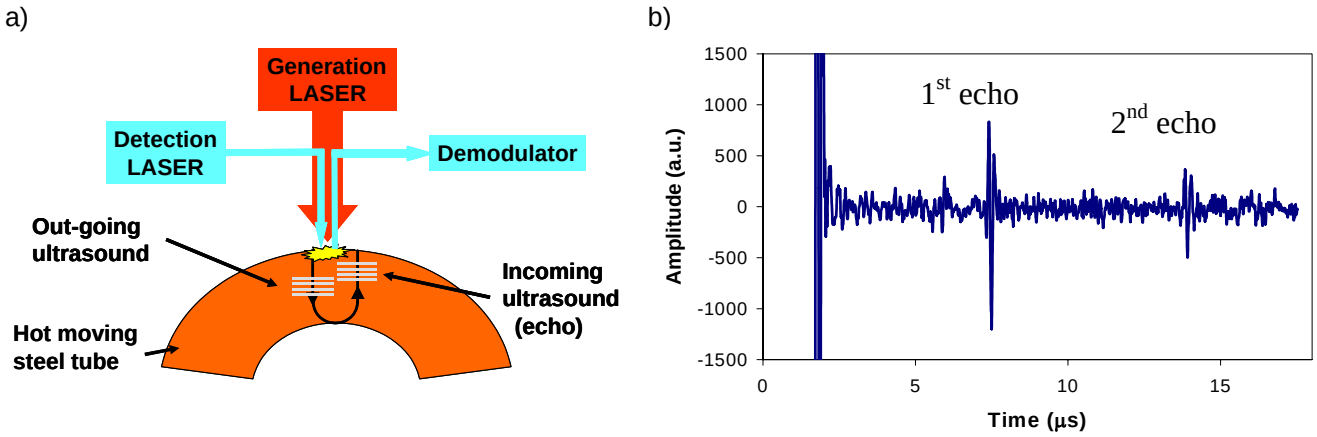

Figure 1. a) Principle of laser-ultrasonic generation and detection in a tube and b) signal acquired on-line for a 16 mm thick steel tube at 940°C.

3. Tube wall thickness measurement

For determination of wall thickness, a signal processing approach based on a single echo was developed to measure time-of-flight (TOF) from the acquired laser-ultrasonic signals in the presence of ultrasonic backscattered noise. Numerical cross-correlation is performed between the first ultrasonic echo reflected from the inner surface of the tube and a reference pulse. The cross-correlation technique, an optimal matched-filter, traditionally uses two successive echoes in the signal and has shown success in determining precise TOF with sufficiently high signal-to-noise ratio (SNR) of the second echo [7]. Such a second echo may be too weak in laser-ultrasonic signals from hot seamless steel tubes. As reference pulse, a synthetic pulse is built taking an average of several signals and fitting the obtained pulse with a model of the pulse.

The use of split spectrum processing (SSP) for the case of very low SNR was also considered. SSP consists in the decomposition of a signal into multiple signals by applying a set of narrow band Gaussian filters. The set of signals is then processed with a non-linear operator to yield a composite signal having a better SNR. For a given non-linear operator, the efficiency of SSP depends on three parameters: the filter width, the filter separation and the number of filters. It as been shown that optimum values of the filter width and filter separation can be found [8]. The optimum value for the number of filters is more complicated, but is related to the effective frequency bandwidth of the ultrasonic echoes. Therefore, after proper windowing of the echo and the reference as input to cross-correlation, a strategy was implemented to use SSP on the cross-correlation output. Considered as matched-filter, the cross-correlation result should strengthen the coherent part of the original signal and SSP could help locating the true maximum in the cross-correlation output to determine the TOF.

Figure 2 shows an example of using the single-echo approach described above from a signal having a low SNR. On the left, the signal on top is the reference pulse and the signal between cursors on bottom is used for interrogation of the first echo. Notice that the horizontal axis is the time in μs and that the amplitude of each signal is normalized to one. On the right, the result from cross-correlation is shown on top, the horizontal axis being the time lag with respect to the beginning of each signal portions. Also, the result from SSP is shown on bottom, which clearly indicates the presence of a coherent signal in the cross-correlation output. We have observed that in many occasions the signal has a sufficient SNR to avoid the additional step of performing SSP on the cross-correlation output. The wall thickness is then determined from the TOF using the ultrasonic velocity at given measurement location with the temperature given by the pyrometer. Also, eccentricity can be determined from several wall thickness values around the tube circumference using a statistical estimator.

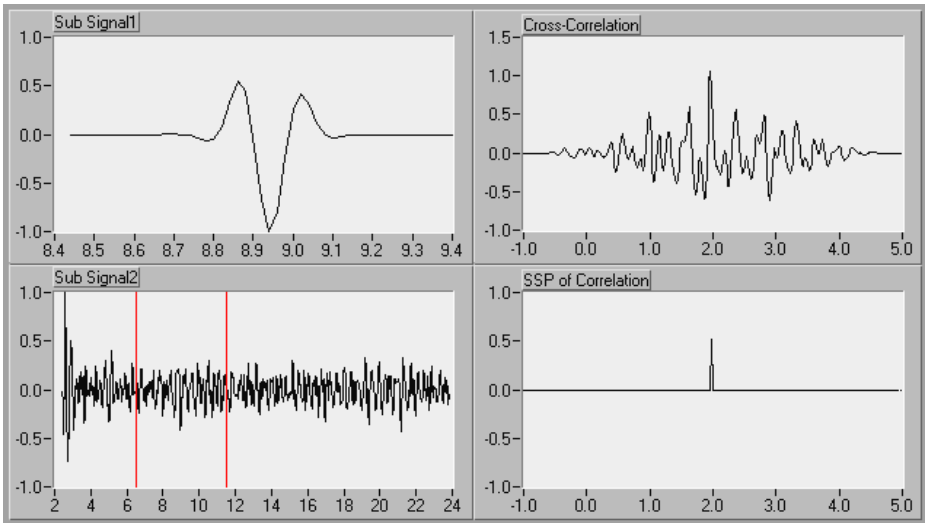

Figure 2. Example of cross-correlation with SSP on the first echo of a signal having a low SNR.

Accuracy of the system in gauging hot tubes properly was verified by selecting several tubes and measuring them at room temperature with a conventional ultrasonic gauging system. The results obtained at high and room temperatures were found in very close agreement (within +/- 0.5%). The system providing in real-time wall thickness information over the whole tube length allows adjustment of the mill to get a product within specifications. It also allows detecting worn or defective mechanical parts of the mill. Figure 3 presents one example of corrections that were made possible with a tube that was out-of-specifications except at its very ends. Without the system, using the conventional method of cutting from time-to-time tube endings and manually measuring them, such defective tubes would have

been processed with exceeding wall thickness unnoticed, resulting in additional costs for additional machining.

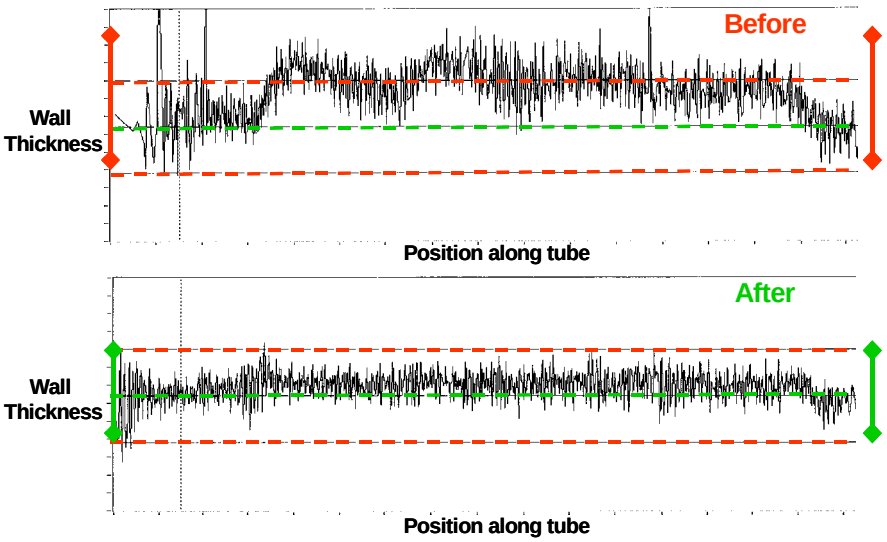

Figure 3. Example of a tube detected within specification only at its very ends and then, after corrective measures brought to the line, the next tube produced within specifications along the entire length.

4. Austenite grain size measurement

For determination of austenite grain size, a signal processing approach also based on a single echo was developed to obtain a relative attenuation spectrum from laser-ultrasonic signals in the presence of backscattered noise. The approach was used to quantitatively determine austenite grain size over a wide range (20 to 300 μm) and for relatively thick materials (up to 30 mm). The method consists in proper windowing of the first echo and calculation of its amplitude spectrum for both the signals from the tube and from a reference material. The frequency-dependent attenuation curve is then calculated by the ratio between the spectrum of the reference and that of the tube material to be characterized. A scattering parameter, b, related to austenite grain size is determined by fitting the experimental attenuation curve to a model for the attenuation mechanisms involved such as:

$$\alpha(f) = \alpha_o + af^m + bf^n \qquad (1)$$

where m and *n* are the frequency powers, respectively for absorption and scattering. According to well accepted models for these mechanisms, m is between 0 and 2 and n is between 0 and 4. For robustness, m and n could be kept fixed during fitting, and should not be too close. Otherwise, a single power-law term should be used with an effective frequency power for both mechanisms involved. Then a calibration curve is established between the scattering parameter and the austenite grain size measured by metallography on many steel samples. Figure 4 illustrates the method showing an example of the material and reference echo spectra, and the resulting ultrasonic attenuation measured and fitted with a model. In this approach, the normalization by a reference material signal allows the correction for system response and diffraction but does not take into account fluctuations in signal strength from one measurement to another. Normalization for such variations is made unnecessary by fitting the experimental attenuation curve to a model that accounts for this, e.g. including a constant factor α_o as in Eq. (1). This method is particularly efficient for broadband ultrasonic systems with sufficiently good response as low frequencies.

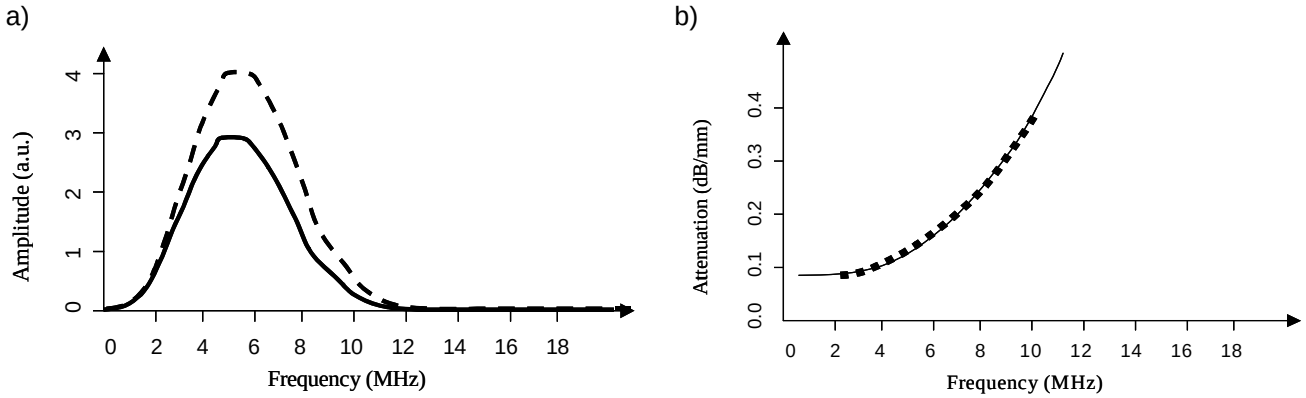

Figure 4. a) Example of the material (solid line) and reference (dashed line) spectra, and b) resulting attenuation spectrum measured (dots) and fitted (line) with a model.

For calibration, steel samples of different grades were heated in a Gleeble thermomechanical simulator in the range of 900 to 1250 °C and held to saturate grain growth. During the whole thermal cycle, laser-ultrasonic measurements were performed and, after proper quenching (varying with the steel grade), the former austenitic grains were revealed by etching and quantitatively characterized by image analysis. Measurements were also performed on a reference sample of steel having low attenuation to obtain the attenuation spectra. Figure 5a depicts an example of a calibration curve, where the scattering parameter, b, obtained from fitting the attenuation spectrum of the first echo is plotted against the grain size obtained from metallography. For on-line measurements, many challenges specific to such conditions were addressed. To improve the attenuation spectrum quality, ultrasonic signals obtained at many positions along the tube are averaged, and the grain size is evaluated over a segment of the tube or over the whole tube. Also, the effects of tube eccentricity and roughness were found to be somewhat small and no correction was applied. Figure 5b shows the comparison between austenitic grain size measured on-line by the laser ultrasonic system and that obtained by metallography on the same tubes after proper quenching. Due to the on-line conditions, the ultrasonic measurements are expected to be less accurate that those performed in the laboratory. The metallographic values are also less accurate due to the challenge of applying, in the production environment, the proper cooling procedure that allows the visualization of former austenitic grain sizes. With estimated metallographic grain size accuracy between 0.5 and 1 ASTM, a statistical analysis shows that the laser-ultrasonic grain sizes determined on-line have at least the same accuracy as those obtained from standard metallography methods.

5. Conclusion

A laser-ultrasonic system was developed and implemented to gauge thickness and determine the austenite grain size on-line in a seamless tube production plant. A signal processing approach based on a single echo is used in the presence of backscattered noise and moderately low SNR after propagation in relatively thick materials. This system also includes a pyrometer to measure tube temperature and a coordinate measuring system to determine the measuring locations. This system provides thickness information all along the tube length unlike the conventional technique of cutting and measuring end sections. It eliminates such an imprecise and tedious practice and contributes to increased productivity. The real-time determination of the austenitic grain size provides an extraordinary tool towards controlling microstructure by a closed loop controlled thermo-mechanical processing. A statistical analysis with metallographic results shows that the laser-ultrasonic grain sizes determined on-line have at least the same accuracy. With more than 1,000,000 tubes inspected since its March 2002 deployment, the system has demonstrated its reliability and usefulness and is leading to significant productivity increase.

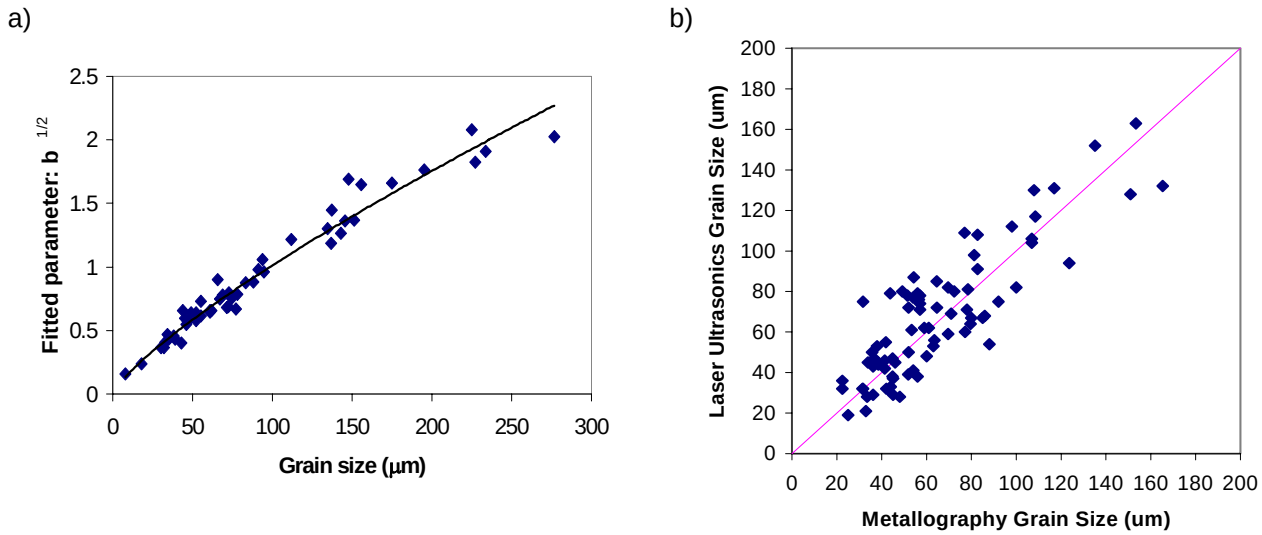

Figure 5. a) Calibration of the fitted attenuation parameter 'b' and metallographically measured austenite grain size. b) Austenite grain sizes measured on-line by the laser ultrasonic system as a function of those obtained by metallography on the same tubes after proper quenching.

6. Acknowledgments

This work was partially supported by the Department of Energy under Award No. DE-FC07-99ID 13651 and DE-PS07-99ID 13750.

REFERENCES

[1] Scruby (C.B.) and Drain (L.E.). - *Laser-Ultrasonics: Techniques and applications*, Adam Hilger, Bristol, UK, 1990.

[2] Monchalin (J.-P.), Néron (C.), Bussière (J.-F.), Bouchard (P.), Padioleau (C.), Héon (R.), Choquet (M.), Aussel (J.-D.), Carnois (C.), Roy (P.), Durou (G.), Nilson (J.A.). - *Laser-ultrasonics: from the laboratory to the shop floor*, Advanced Performance Materials 5, p. 7-23, 1998.

[3] Paul (M.), Hoffman (A.), Deppe (G.J.) and Oesterlein (L.). - *Laser ultrasonics in industry*, Proc. of the 7th European Conference on Nondestructive Testing, Copenhagen, May 26-29, p. 2134-2141, 1998.

[4] Keck (R.), Kruger (B.), Coen (G.) and Hasing (W.). - *Wandickenmeassung an 1230C heissen Rohrluppen mit enem neuartigen Laser-Ultrashall-System*, Stahl und Eisen 107, p. 1057-1060, 1997.

[5] Dubois (M.), Militzer (M.), Moreau (A.) and Bussiere (J.-F.). - *A New Technique for the Quantitative Real-Time of Austenite Grain Growth in Steel*, Scripta Materialia 42, p. 867-874, 2000.

[6] Monchalin (J.-P.), Choquet (M.), Padioleau (C.), Néron (C.), Lévesque (D.), Blouin (A.), Corbeil (C.), Talbot (R.), Bendada (A.), Lamontagne (M.), Kolarik II (R.V.), Jeskey (G.V.), Dominik (E.D.), Duly (L.J.), Samblanet (K.J.), Agger (S.E.), Roush (K.J.) and Mester (M.L.). - *Laser Ultrasonic System for On-Line Steel Tube Gauging*, Review of Progress in Quantitative NDE, Vol. 22, eds. D. O. Thompson and D. E. Chimenti, AIP, New York, p. 264-272, 2003.

[7] Aussel (J.-D.) and Monchalin (J.-P.). - *Precision laser-ultrasonic velocity measurement and elastic constant determination,* Ultrasonics 27, p. 165-177, 1989.

[8] Aussel (J.-D.). - *Split spectrum processing with finite impulse response filters of constant frequency-to-bandwidth ratio*, Ultrasonics 28, p. 229-240, 1990.

Proc. Vth International Workshop, Advances in Signal Processing for Non Destructive Evaluation of Materials
Québec City (Canada),2-4 Aug. 2005. © X. Maldague ed., É. du CAO (2006), ISBN 2-9809199-0-X

QUÉBEC 2005 Best Presentation Award Paper

Lockin-ESPI interferometric imaging for remote non-destructive testing

H. Gerhard and G. Busse

Institute for Polymer Testing and Polymer Science (IKP) – Department of Non-Destructive Testing, Stuttgart University, Pfaffenwaldring 32, D-70569 Stuttgart, Germany

Abstract
Electronic-speckle-pattern-interferometry (ESPI) is a sensitive interferometric imaging technique that responds to changes of surface topography caused e.g. by pressure changes or by thermal expansion. Hidden defects are revealed by the inhomogeneity of such deformation fields. Unfortunately, field distortion may also be caused by e.g. inhomogeneous excitation. Therefore the lockin technique has been transfered to ESPI in order to enhance its sensitivity by this kind of phase-sensitive narrow-band filtering where finally a self-normalised phase-angle image is obtained. Such an image displays features which are usually deeply hidden in noise, as will be shown on various examples.

Key words: Interferometry, ESPI, Non-destructive Testing, NDE, Lockin, deformation modulation

1. Introduction

Interferometric imaging is a well established technique that responds to changes of surface topography and displays the result as a fringe pattern. The principle behind this is the fact that similar patterns superposed to each other display a spatial beat pattern, very similar to the one that can be observed occasionally on highway bridges where one periodical structure is closer to the eye thereby having a seemingly different periodicity. Superposition of them results in a one-dimensional beat pattern (“Moiré-effect”) whose periodicity is related to the difference of the structures (Fig.1).

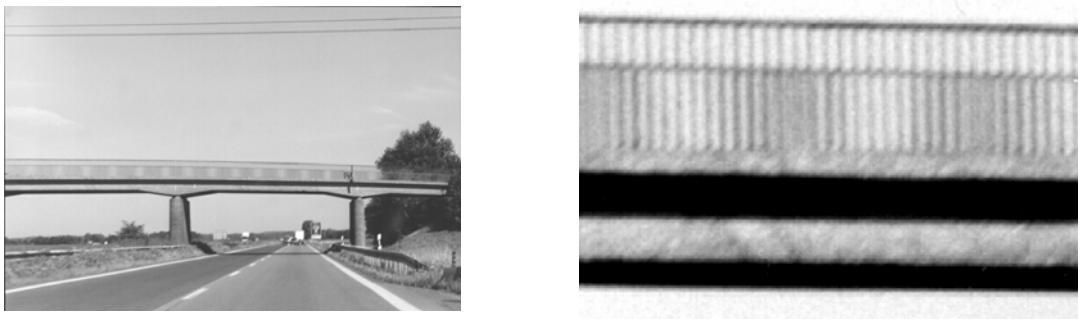

Figure 1: Moiré-effect on a bridge.

If an object is imaged by a camera in laser light and a reference beam (derived from the laser directly or from the object under a different angle) superposed, the resulting image has a grainy structure (“speckles”) since the superposition causes interference effects [1]. Therefore these speckles respond in a sensitive way to tiny changes of the object shape. If two such images are superposed that have been taken at different states of deformation (induced e.g. by load or thermal expansion]), again a Moiré-pattern is observed, but this time in a two-dimensional arrangement and not in just one dimension. A convenient example to demonstrate this effect is the growth of

champignons whose flat white surface with its light-scattering properties is well suited for interferometric imaging (Fig.2). If two images are taken with 5 seconds in between, the small structural change due to growth results in fringe formation. Like on a map these are contour lines, but instead of height itself they display the hight change that occurred between the two states of deformation. The hight difference between two contour lines is half the laser wavelength. Hight direction is in this case along the optical axis of the setup ("out-of-plane image"). With a laser wavelength of about 0.8 µm and observed three fringes the champignon radius has obviously changed by 1.2 µm.

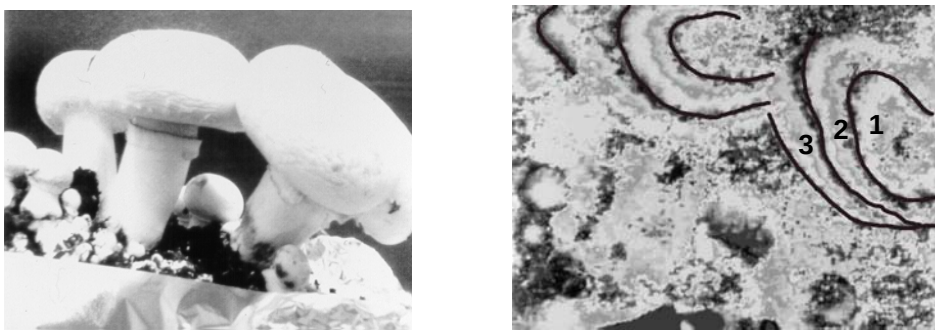

Figure 2: Photography of champignon group (left). Out-of-plane ESPI-image (right) of growth within 5 seconds. 3 Fringes indicated by black lines for better clarity.

Of course this change is an increase, but shrinkage would provide about the same pattern. This ambiguity is eliminated if the images are not simply superposed but the optical path length varied in e.g. four steps each by a quarter of the laser wavelenth (by a mirror mounted on a piezo translator) so that the mathematics can be improved in such a way that the local difference phase angle is determined. It should be emphasized that the highly contrasted contour lines in such a "modulo 2π image" display the optical interferometric phase [2]. The mathematics involved in deriving the phase contain ratioed intensity differences, therefore confusing local variations of optical properties cancel in this self-normalisation, so they affect only the noise level. The sign of the steady change within each fringe shows whether shrinkage or growth occurred between the two images, it also reduces noise and allows to convert the phase angle pattern into a continuous high pattern. This advantage becomes obvious in Fig.3 where the difference between two deformation states of a circular plate is presented together with the profile of change finally demodulated from the modulo 2π image [3].

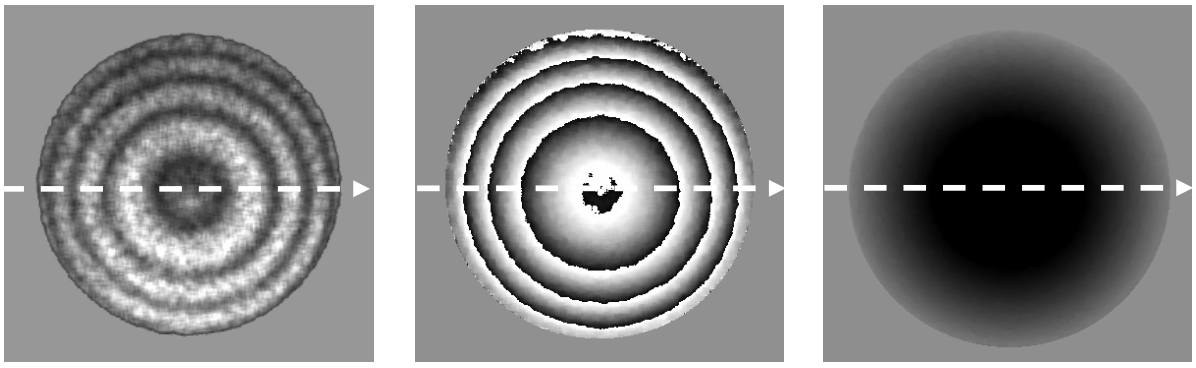

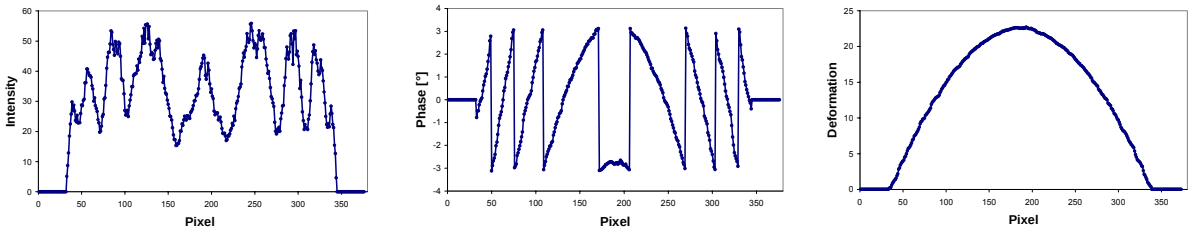

Figure 3: Top: Subtracted image (left), modulo 2π image (middle), and demodulated phase image (right). Bottom: Signal profiles taken along diametral dashed lines of these images.

While in this example the deformation mechanism has been built in by nature, technical materials need external excitation to change their shape. As interferometric imaging is sensitive to perturbations, a tensile test requires special care. Therefore it is simpler to expose the sample to light which is absorbed thereby heating the object so that it expands thermally. The contour pattern displays again lines of equal deformation. The main topic of interest for nondestructive evaluation (NDE) is then how such lines deviate from the expected pattern e.g. due to hidden defects which can be identified this way.

2. Phase sensitive ("Lockin") interferometric imaging

2.1. Principle

In this conventional setup for interferometric imaging the total change of shape is monitored while one is interested only in the small changes caused by hidden defects. In this context it is of interest to note that the dynamic range of such images is rather limited. The way to solve this problem is transfered from lockin-thermography [4-7] or generally from dynamic measurement techniques: The effect to be investigated is modulated while a sequence of images is taken which is then Fourier-transformed at the frequency of deformation modulation. In this weighted averaging of images the frequency bandwidth of noise is reduced so that a considerable improvement of the signal to noise ratio is achieved. Additionally, this phase-sensitive narrow band filtering provides at each pixel the local phase of response with respect to the modulated input (not to be confused with the optical phase described above) which is again insensitive to locally changed degrees of modulation (e.g. illumination by the lamp used for remote heating).

This technique is applicable generally to every deformation component (in-plane or out-of-plane) of interferometric imaging [8], e.g. to shearography where the gradient of the deformation field is monitored or to speckle interferometry which responds to the deformation field directly. However, in the following we restrict ourselves to the out-of-plane component of Electronic-Speckle-Pattern-Interferometry (ESPI) in order to demonstrate the principle ("Lockin-ESPI"). The word "Lockin" is being used to illustrate that the principle corresponds to the hardware lockin-amplifier being around since many decades to analyse amplitude of a modulated signal with respect to a reference input. Such a lockin-function is related to each pixel of the interferometric image [9, 10].

To do that, one step has to be performed that makes a big difference as compared to other lockin-methods: The fringe patterns have first to be converted to maps of height change and then the Fourier transformation of height modulation is performed at each pixel of the sequence. In this context the word "demodulation" can be used twice: Once to describe the procedure converting contour maps into height, and then again to derive from the sequence of images finally an image displaying amplitude and phase of the modulation effect at each pixel. This way the whole information contained in many images is finally compressed into just two: an amplitude image and a phase image. The latter one is more useful: The overall bending of a component occurs everywhere at the same time, so it has the same phase angle which gives a constant background. A defect is an area where heat propagation and hence the time constant of deformation can be modified hence

giving a different phase. So the result is that such a defect stands out clearly against an otherwise constant background which is a big advantage as compared to the amplitude image where the tiny additional bump caused by the defect needs to be detected in the presence of the potentially heavily structured background caused by the intact structure. Examples illustrating this important difference will be shown later on.

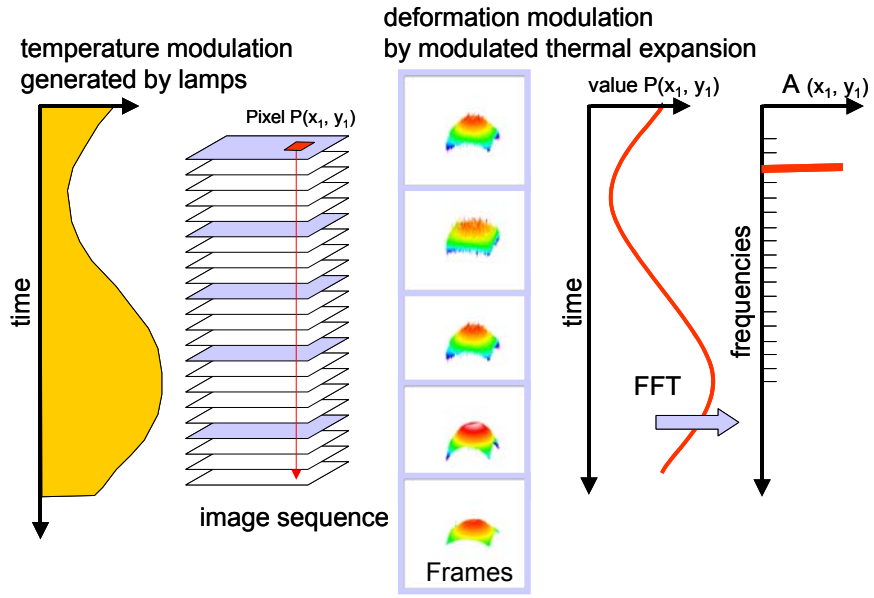

Figure 4: Determination of amplitude image A from the sequence. Phase is determined from the same Fourier transformation.

2.1.Measurement set-up

For the investigations decribed below we used a small home made out-of-plane ESPI set-up where wavelength of the 75mW laser was 532nm.

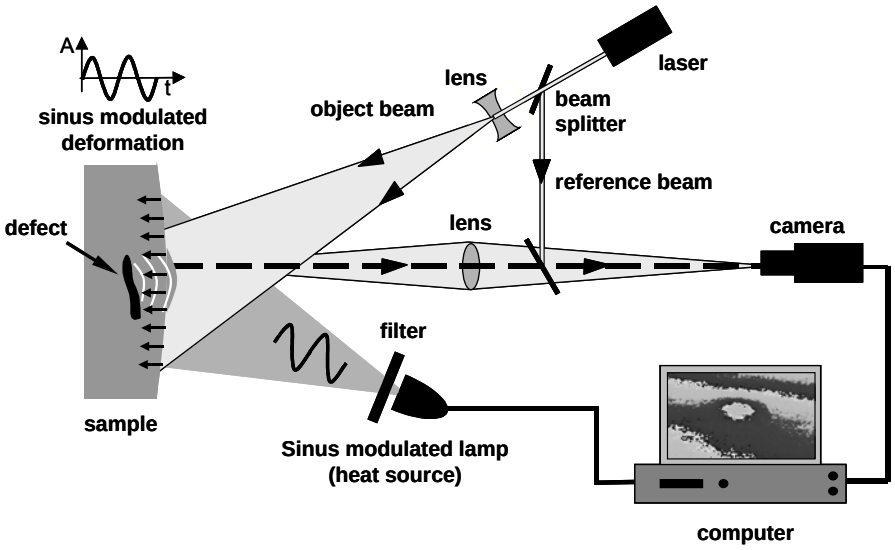

Figure 5: Basic setup of Optical Lockin ESPI (OLI) [9].

For modulated heating we used four 1000W lamps whose power was computer controlled and synchronised to the rate at which the sequence of optical phase images (each resulting from 4 piezo shifted single images) were taken. For clarity it should be mentioned that optical intensity on the sample was less than the one of sunshine in summer. Then all images were unwrapped/demodulated to hight and then Fourier transformed at the modulation frequency which ranged between 0.01Hz and 1Hz. The depth into which the temperature modulation propagates is given by the thermal diffusion length μ with

$$\mu = \sqrt{\frac{2\alpha}{\omega}}$$

where α denotes thermal diffusivity and ω the angular frequency of lamp modulation [11]. The frequency dependence provides an efficient tool for depth range variation, as is known since some time from thermal wave applications [11-16].

3. Experimental results

3.1. Simulated defects in a PMMA plate

The applicability of this new technique is demonstrated on a circular PMMA-sample provided with a subsurface hole in the center (Fig. 6) to simulate a hidden defect. The surface of the transparent sample was painted with black color in order to avoid selective defect heating. After applying the procedure described above it turns out that the amplitude image has a curved structure where the effect of the hole is hidden while the phase image is mostly flat so that the simulated defect stands out clearly.

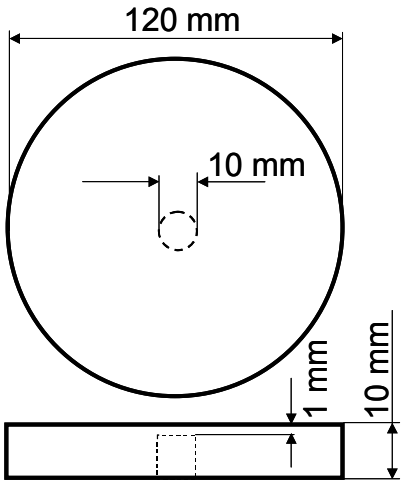

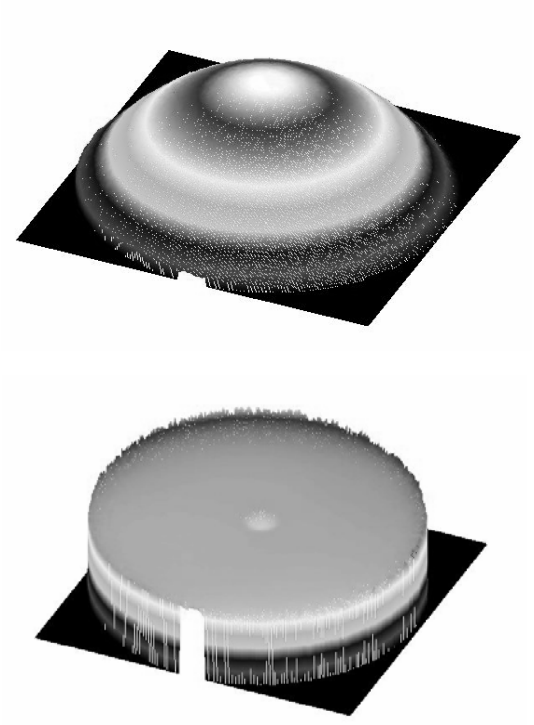

Figure 6:
Left: Geometry of specimen
Right: Amplitude (top)
and phase image (bottom)

Some images of the sequence from which the two images in Fig. 6 were derived are shown in Fig. 7. The simulated defect disappears in noise, it is revealed by the narrowband filtering process. The final limitation of the method seems to be convection and the related change of the refractive index which is modulated at the lamp frequency, therefore it is not eliminated by the Fourier-

transformation. Comparative measurement were performed where convection was tentatively reduced. The achieved improvement of signal to noise is obvious (Fig. 8).

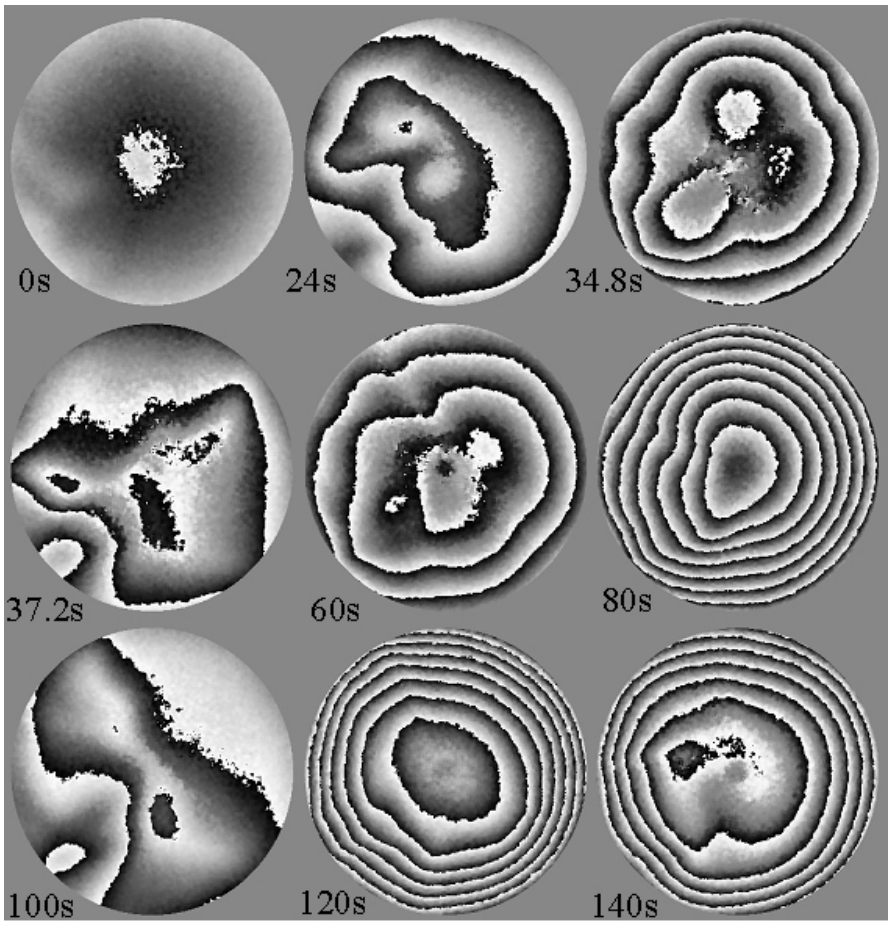

Figure 7: Some images from time sequence obtained on a PMMA sample.

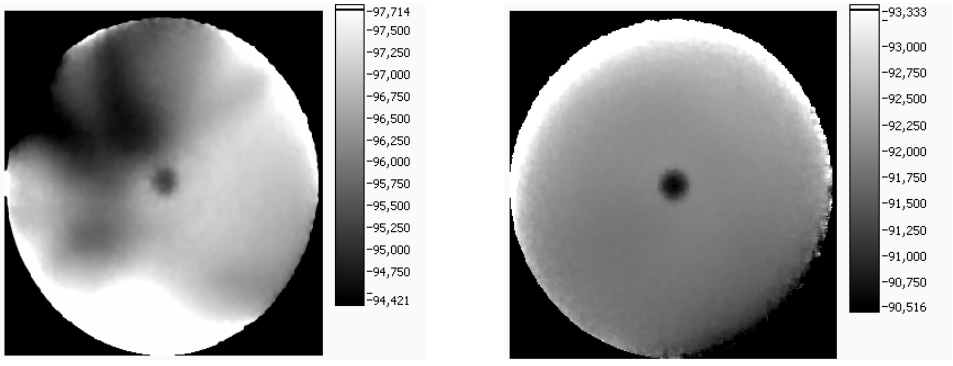

Figure 8: Phase images analysed by a modulation frequency at 0.04Hz.
Measurement influenced by refraction index (left),
reduction of refraction index (right).

In another experiment we investigated how defect detectibility depends on modulation frequency. This influence is expected since the depth of modulated heating depends on thermal diffusion length which becomes smaller when the frequency increases [11]. Fig. 9 confirms this relation: The hidden defect is detected only if modulation is 0.15 Hz or lower. Therefore depth profiling is basically possible with Lockin-ESPI.

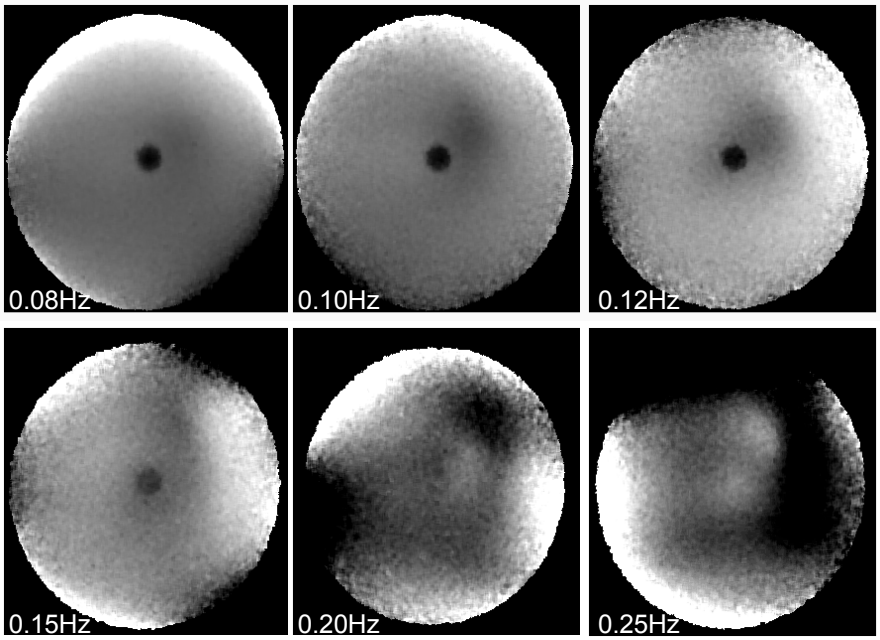

Figure 9: Phase images obtained with Lockin-ESPI at several frequencies.

3.2 Depth resolved measurements in wood

To investigate the influence of modulation frequency on depth range we performed measurements on the wood sample described previously [9] with holes hidden under a layer of veneer (to simulate disbonds) in a matrix arrangement where hole diameter changes along one direction and the thickness of veneer along the other. The reason for this choice of material is that wood is a natural material which is important for furniture where genuine wood is used only for the veneer layer while cheaper material is being used for the core. Disbonds between veneer and substrate can be detected using OLI. In order to investigate this potential we performed measurements between 0.03 and 0.09 Hz. In Fig. 10 the hole diameter decreases from top to bottom while the veneer thickness increases from 0.5mm (left) to 2.5mm (right). At 0.09Hz the holes are detected only if the veneer layer is thinner than 1.5mm. By frequency reduction the penetration depth of the thermal waves increases and allows to detect holes under 2.5mm. This example shows the potential for remote depth profiling of defects.

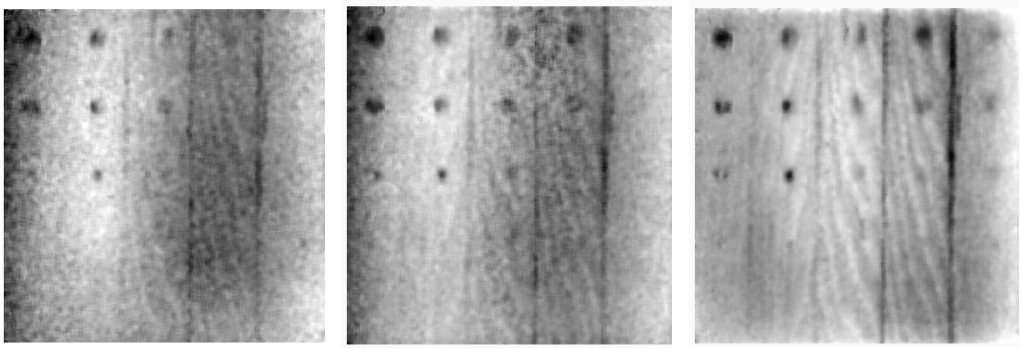

Figure 10: Depth resolved measurements of holes under different veneer thicknesses (sample kindly manufactured by Mr. Koppenhöfer, trade school Schwaebisch-Hall / Germany).

3.3. Comparison between Lockin-ESPI and optcally excited Lockin-thermography

Though this result is very much similar to what is known from lockin thermography, it should be mentioned that the experience cannot be simply transferred to lockin ESPI since signal generation does not only depend on the thermal wave but additionally on thermal expansion and related strain fields. We performed experiments aiming at a comparison between lockin-thermography and lockin-ESPI. In order to see the hidden structure (which was again covered by paint for the experiments) we used a PMMA sample where 4 holes were drilled parallel to the surface at a depth of 1 mm. Three holes were subsequently filled with metal cylinders (copper, aluminum, steel) pressed into them while the fourth hole was empty for reference (Fig. 11).

Measurements were performed at 0.1 Hz modulation frequency of the lamps used for modulated heating. Comparison shows:

The holes appear narrower with Lockin-thermography. The point-spread-function is broader for Lockin-ESPI which is obvious since the strain fields extend further than the thermal wave field [15,17].

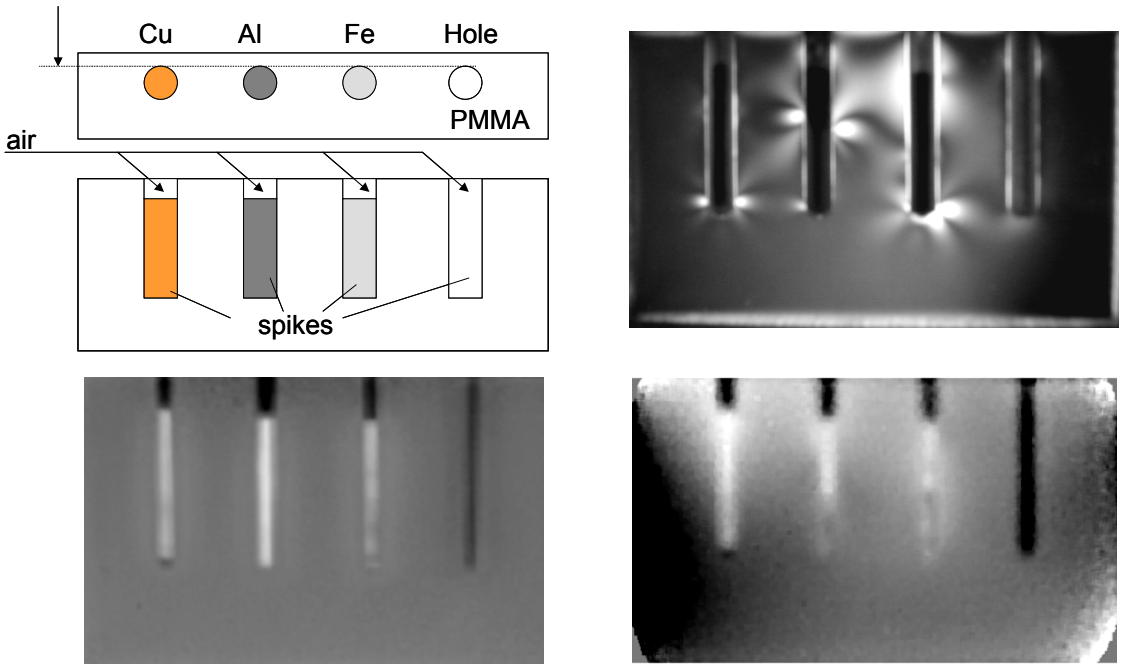

Figure 11: PMMA-specimen with four 5mm diameter subsurface holes (left top) with hole axis parallel to the illuminated surface. Lockin-thermography phase image at 0.1Hz (left below –recorded by Mr. Gleiter, IKP) Lockin-ESPI phase image at 0.1Hz (right below), and stress distribution displayed by photoelasticity (right top).

The lower part of the inserted steel and aluminum cylinders differs from the upper part in the Lockin-ESPI-image while such a difference is not found in the Lockin-thermography image which does not respond to the superposed strain field. Therefore the conclusion is that the strain field causes the observed difference. This argument is supported by results of photoelasticity measurements performed in transmission after the paint was removed from the sample surface: The two cylinders in the middle have a strong structure around them indicating inhomogeneity of stress. From this result on PMMA we conclude that Lockin-ESPI responds to stress fields also in opaque samples which is very important for industrial applications.

3.4 Lockin-ESPI for defect detection in honeycomb plate

Results obtained from basic research should be applicable to real-life samples, e.g. honeycomb structures whose high specific stiffness is of interest for aerospace applications. The critical part of such structures is where the skin is bonded to the core. Ingress of water or excessive glue may result in stiffness reduction or too much weight, respectively. In our investigations we used a honeycomb structure (420x170x13mm³) partially filled with glue. Additionally, a marking strip is visible in the middle of the plate.

The single images of optical phase taken from the whole sequence (one of them shown in Fig.12) vary during modulation with no indication of structure. The information extracted by Fourier transformation at the lamp modulation frequency 0.06 Hz is again compressed into an amplitude image and a phase image of local modulation. Obviously the phase angle image contains the relevant information: The two circular areas of modified stiffness stand out clearly in the lockin phase image (Fig.12 right) derived from the sequence at the frequency of excitation while they are hidden in the strong background deformation in each single image of the sequence.

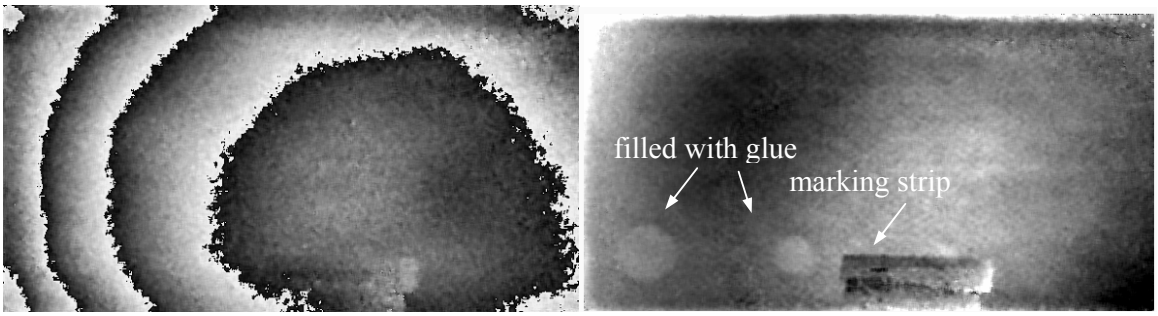

Figure 12: One wrapped interferometric phase image of the sequence (left).
Lockin phase image from Fourier transformation of sequence at 0.06Hz [18] (right).

4. Conclusions

Lockin-ESPI is an improved version of the well known ESPI-technique. It responds only to modulated changes of topography induced e.g. by thermal expansion due to absorption of modulated radiation. The result is a significant enhancement of the signal to noise ratio in the imaging of defect. As the overall deformation of the surface is suppressed the probability of

detection (POD) is much enhanced. Also depth analysis of the defects is possible by variation of the lockin frequency.

Further developments to be transferred from other techniques are obvious: Instead of performing depth analysis by subsequent measurements at different frequencies one can as well use burst excitation (containing a broad frequency spectrum) and transform just one obtained sequence at various frequencies. Also, nonlinearities can be investigated by analysing the sequence at overtone frequencies as a response to monofrequency sinusoidal input. Such images would display selectively defects (e.g. clapping of disbonds).

In that sense this paper can be considered as a first feasibility investigation that explores the potential of a widely applicable new technique expanding the scope of applications for interferometric imaging in the field of remote NDE.

REFERENCES

[1] Jones, R.; Wykes, C.: Holographic and Speckle Interferometry. A discussion of the theory, practice and application of the techniques. Cambridge: Cambridge University Press, 1983

[2] Cloud, G.: Optical Methods of Engineering Analysis. Cambridge: University of Cambridge, 1995

[3] Ghiglia, D.; Pritt, M.: Two-Dimensional Phase Unwrapping: Theory, Algorithms, and Software. Wiley, New York, 1998

[4] Carlomagno, G.; Berardi, P.: Unsteady thermotopography in non-destructive testing. In: Proc. 3nd Biannual Exchange, St. Louis/USA, 24.-26. August 1976, pp.33-39

[5] Beaudoin, J. L.; Merienne, E.; Danjoux, R.; Egee, M.: Numerical system for infrared scanners and application to the subsurface control of materials by photothermal radiometry. Infrared Technology and Applications SPIE Vol.590, 1985, p. 287

[6] Kuo, P. K; Feng, Z. J.; Ahmed,T.; Favro L. D.; Thomas, R. L.; Hartikainen, J.: Parallel thermal wave imaging using a vector lock-in video technique. In: Photoacoustic and Photothermal Phenomena (Hrsg. P. Hess and J. Pelzl). Springer-Verlag, Heidelberg 1987, pp. 415-418

[7] Busse, G.: Lockin thermography. Nondestructive Testing Handbook. Vol 3: Infrared and Thermal Testing (Ed. X. Maldague). American Society for Nondestructive Testing Inc., Columbus,OH, 2001, pp. 318-327, ISBN 1-57117-044-8

[8] Patent DE 4203272- C2, 1992

[9] Gerhard, H.; Busse, G.: Use of ultrasound excitation and optical-lockin method for speckle interferometry displacement imaging. In: Green, R.E. Jr.; Djordjevic, B.B.; Hentschel, M.P. (Eds): Nondestructive Characterisation of Materials XI, Springer-Verlag Berlin, 2003, pp. 525-534, ISBN: 3-540-40154-7

[10] Gerhard, H.; Busse, G.: Zerstörungsfreie Prüfung mit neuen Interferometrie-Verfahren. In: Materialprüfung, Vol. 45 Nr. 3, 2003, pp. 78-84

[11] Rosencwaig, A.; Gersho, A.: Theory of the photo-acoustic effect with solids. J. Appl. Phys., 1976, pp. 64-69

[12] Busse, G.: Optoacoustic phase angle measurement for probing a metal. In:Appl. Phys. Lett. Vol. 35, 1979, pp.759-760

[13] Rosencwaig, A.; Busse, G.: High resolution photoacoustic thermal wave microscopy. Appl. Phys. Lett. 36, 1980, pp. 725-727

[14] Opsal, J.; Rosencwaig, A.: Thermal wave depth profiling: Theory., J. Appl. Phys. 53, 1982, pp. 4240-4246

[15] Busse, G.; Rosencwaig, A.: Thermal wave piezoelectric and microphone detection for non-destructive evaluation: a comparison. In: J. Photoacoustics 1, 1983, pp. 365-369

[16] Maldague, X.; Krapez, J.C.; Cielo, P.; Poussart, D.: Inspection of materials and structures by infrared thermography: signal processing techniques for defect enhancement and

characterization., Canadian Society of Nondestructive Testing Journal, 10 [1], pp. 28-36, 1989

[17] White, R.M.: Generation of elastic waves by transient surface heating. In: J. Appl. Phys. 34, 1963, pp.3559-3567

[18] Gerhard, H.; Busse, G.: Two new techniques to improve interferometric deformation-measurement: Lockin and Ultrasound excited Speckle-Interferometry. Proc. Fringe 2005, Ed. W. Osten, Springer-Verlag Berlin, 2005, pp.530-538, ISBN: 3-540-26037-4